Journal of Coordination Chemistry

ISSN: 0095-8972 (Print) 1029-0389 (Online) Journal homepage: http://www.tandfonline.com/loi/gcoo20

Cobalt and nickel coordination polymers containing 3-pyridylnicotinamide and five-membered ring dicarboxylates

Maria D. Torres Salgado, Caitlin J. Bouchey, Julie A. Wilson & Robert L. LaDuca

To cite this article: Maria D. Torres Salgado, Caitlin J. Bouchey, Julie A. Wilson & Robert L. LaDuca (2015) Cobalt and nickel coordination polymers containing 3-pyridylnicotinamide and five-membered ring dicarboxylates, Journal of Coordination Chemistry, 68:11, 2029-2040, DOI: 10.1080/00958972.2015.1038997

To link to this article: http://dx.doi.org/10.1080/00958972.2015.1038997

Journal of Coordination Chemistry, 2015
Vol. 68, No. 11, 2029–2040, http://dx.doi.org/10.1080/00958972.2015.1038997

Cobalt and nickel coordination polymers containing 3-pyridylnicotinamide and five-membered ring dicarboxylates

MARIA D. TORRES SALGADO, CAITLIN J. BOUCHEY, JULIE A. WILSON and ROBERT L. LADUCA*

Lyman Briggs College and Department of Chemistry, Michigan State University, East Lansing, MI, USA

(*Received 24 July 2014; accepted 24 February 2015*)

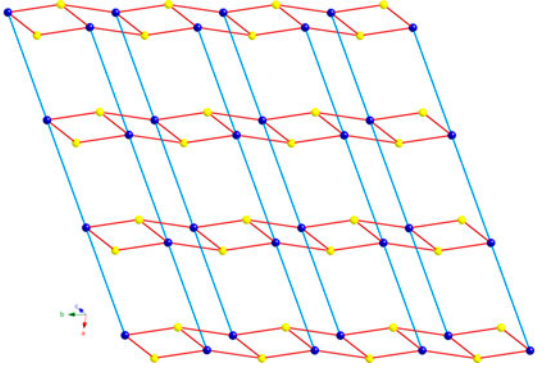

Cobalt and nickel coordination polymers containing the conformationally flexible 3-pyridylnicotinamide (3-pna) ligand and a five-membered ring-based dicarboxylate ligand have been prepared and structurally characterized via single-crystal X-ray diffraction. $[Co(tpdc)(3\text{-pna})]_n$ (**1**) was prepared using 2,5-thiophenedicarboxylic acid (H_2tpdc). This material shows a 2-D layer structure containing $\{Co_2(OCO)_2\}$ dimers linked by tpdc and 3-pna ligands. Compound **1** manifests an underlying 3,5-connected $(4^26)(4^26^78)$ 3,5L2 topology. The isostructural pair of solids $[Co(D\text{-cam})(3\text{-pna})(H_2O)_2]_n$ (**2**) and $[Ni(D\text{-cam})(3\text{-pna})(H_2O)_2]_n$ (**3**) was obtained from the chiral *D*-camphorate (*D*-cam) ligand. These two materials possess acentric ribbon coordination polymer motifs. Compound **1** manifests antiferromagnetic coupling concomitant with Kramers doublet formation. Thermal properties of these materials are also discussed.

Keywords: Coordination polymer; Crystal structure; Cobalt; Antiferromagnetism; Acentric

1. Introduction

The design, structure, and physical properties of metal–organic coordination polymers remain in the spotlight of current research owing to abilities to serve as gas storage

*Corresponding author. Email: laduca@msu.edu

materials [1], selective absorbents [2], ion-exchange media [3], heterogeneous catalysts [4], and explosives trace sensors [5]. The esthetic appeal of their underlying molecular topologies provides another rationale for these investigations [6]. Aromatic dicarboxylates such as phthalate [7], terephthalate (tere) [8], or isophthalate (ip) [9] are the most popular ligand choices for the construction of multi-functional coordination polymers, as these impart the structural rigidity and necessary charge balance for solution-phase self-assembly of a stable crystalline solid. A wide scope of coordination polymer topologies can be accessed by varying the metal coordination geometry, dicarboxylate components, and by employing different neutral dipyridine-type coligands [10].

In contrast to other more commonly used dipyridine coligands such as 4,4′-bipyridine (bpy), the simple hydrogen-bonding capable, dipyridylamide ligand 3-pyridylnicotinamide (3-pna, scheme 1) has not been frequently used in the construction of crystalline coordination polymers [11–20]. The dipyridylamide linker has been utilized to prepare coordination polymers containing flexible aliphatic dicarboxylates such as succinate (suc) and glutarate (glu). $\{[Cd(suc)(3\text{-pna})]\cdot 2.5H_2O\}_n$, which formed as a mixture of supramolecular isomers with different carboxylate binding modes, has a 3-D dimer-based non-interpenetrated $4^{12}6^3$ **pcu** network [11], while $\{[Cu(glu)(3\text{-pna})(H_2O)]\cdot H_2O\}_n$ has a simple (4,4) grid-like layer structure featuring isolated copper ions [12]. More recently, we have investigated the preparation of aromatic dicarboxylate coordination polymers containing 3-pna; the zinc terephthalate system proved especially complicated [13]. In the presence of added base, $\{[Zn(tere)(3\text{-pna})_2(H_2O)_2]\cdot 2H_2O\}_n$ was formed under hydrothermal conditions. This material displays 1-D $[Zn(tere)(H_2O)_2]_n$ coordination polymer chains bearing monodentate, pendant 3-pna ligands. Without extra base, a mixture of $\{[Zn(tere)(3\text{-pna})]\cdot 3H_2O\}_n$ and $\{[Zn_4(tere)_3(OH)_2(3\text{-pna})_2]\cdot 2H_2O\}_n$ was obtained. The former possesses a 2-D (6,3) hexagonal grid topology with a very tight interdigitation scheme, while the latter exhibits a twofold interpenetrated 3-D $4^{12}6^3$ **pcu** network built from $\{Zn_4(OCO)_2(OH)_2\}$ tetrameric nodes.

Among possible dicarboxylate ligands containing five-membered rings, 2,5-thiophenedicarboxylate (tpdc, scheme 1) and the chiral *D*-camphorate (*D*-cam, scheme 1) have been employed in self-assembly of coordination polymers in the presence of dipyridine-type coligands. The tpdc ligand is similar to ip, but the strained five-membered aromatic thiophene ring orients the carboxylate groups ~152° apart, 32° wider than the *meta* disposition of carboxylate arms allows in isophthalate [21]. Due to this difference in donor disposition, dual ligand coordination polymers containing tpdc ligands can exhibit different dimensionalities when compared to their ip analogs. By way of example, $[Co(ip)(4,4'\text{-bpy})]_n$ has a (4,4) grid topology constructed from pillared $[Co(ip)]_n$ dimer-based chains [22], while [Co(tpdc)

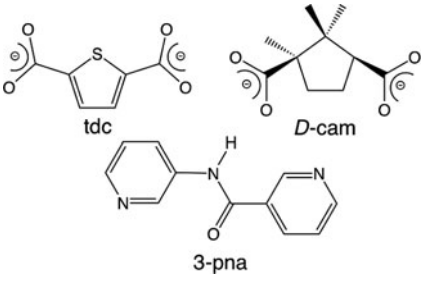

Scheme 1. Ligands used in this study.

$(bpy)]_n$ manifests a twofold interpenetrated **pcu** net built from pillaring of 2-D $[Co(tpdc)]_n$ layer motifs [23].

In regard to coordination polymers containing *D*-cam, $[Ni(D\text{-cam})(dpp)]_n$ (dp*p* = 1,3-di (4-pyridyl)propane) exhibits an extremely rare yet simple 4-connected chiral 2-D bilayer structure with $4^2{\cdot}6^3 8$ topology [24]. $\{[Co(D\text{-cam})(dpp)]\cdot H_2O\}_n$ has a standard, yet chiral, threefold interpenetrated diamondoid net [24], as does its cadmium analog $\{[Cd(D\text{-cam})(dpp)]\cdot H_2O\}_n$ [25]. Dehydration and subsequent heating of the cadmium derivative result in a single-crystal-to-single-crystal structural reorganization. A series of chiral *D*-cam coordination polymers incorporating the hydrogen-bonding capable 4,4′-dipyridylamine (dpa) ligand showed significant structural dependence on the metal ion [26]. The 1-D phase $\{[Cd(dpa)(D\text{-cmphH})_2(H_2O)]\cdot 0.875H_2O\}_n$ exhibits sinusoidal chains with a 67 Å wavelength. $\{[Ni(D\text{-cmph})(dpa)]\cdot 3H_2O\}_n$ exhibits a rare twofold interpenetrated 4-connected $4^2 8^4$ **lvt** topology, but its cobalt congener $\{[Co_2(D\text{-cmph})_2(dpa)]\cdot H_2O\}_n$ shows a dimer-based **pcu** topology.

As there have not yet been any reports of tpdc or *D*-cam coordination polymers containing 3-pyridylnicotinamide, we attempted exploratory experiments toward this goal. Herein, we report the synthesis, crystal structures, and thermal properties of three new coordination polymers containing both 3-pyridylnicotinamide and a five-membered ring-based dicarboxylate ligand: $[Co(tpdc)(3\text{-pna})]_n$ (**1**), $[Co(D\text{-cam})(3\text{-pna})(H_2O)_2]_n$ (**2**), and $[Ni(D\text{-cam})(3\text{-pna})(H_2O)_2]_n$ (**3**).

2. Experimental

2.1. *General considerations*

Metal nitrates and dicarboxylic acids were commercially obtained from Fisher Scientific or TCI America, respectively. The dipyridylamide ligand, 3-pyridylnicotinamide (3-pna), was prepared by the literature procedure [27]. Water was deionized above 3 MΩ–cm in-house. Elemental analysis was carried out using a Perkin Elmer 2400 Series II CHNS/O Analyzer. IR spectra were recorded on powdered samples using a Perkin Elmer Spectrum One DRIFT instrument. Thermogravimetric analysis was performed on a TA Instruments Q50 thermal analyzer under flowing N_2. Variable-temperature magnetic susceptibility data for **2** (2–300 K) were collected on a Quantum Design MPMS SQUID magnetometer at an applied field of 0.1 T. After each temperature change, the sample was kept at the new temperature for 5 min before magnetization measurement to ensure thermal equilibrium. The susceptibility data were corrected for diamagnetism using Pascal's constants, and for the diamagnetism of the sample holder.

2.2. *Preparation of [Co(tpdc)(3-pna)]$_n$ (1)*

$Co(NO_3)_2\cdot 6H_2O$ (81 mg, 0.28 mmol), 3-pna (55 mg, 0.29 mmol), and 2,5-thiophenedicarboxylic acid (48 mg, 0.28 mmol) were mixed with 10 mL of distilled H_2O in a 23 mL Teflon-lined acid digestion bomb. The bomb was sealed and heated in an oven at 120 °C for 48 h, and then was cooled slowly to 25 °C. Magenta blocks of **1** (78 mg, 65% yield based on Co) were isolated after washing with distilled water, ethanol, and acetone and drying in air. $C_{17}H_{11}CoN_3O_5S$ calcd C, 47.67; H, 2.58; N, 9.81%; found C, 47.59; H, 2.80; N,

9.96%. **IR** ($\tilde{\nu}$) = 3249 (w), 3191 (w), 3136 (w), 3077 (w), 2977 (w), 1675(m), 1614 (w), 1589 (w), 1548 (s), 1528(s), 1488 (m), 1472 (m), 1429 (w), 1399 (m), 1372 (s), 1333 (s), 1317 (m), 1305(s), 1265 (w), 1235 (w), 1194 (m), 1122 (w), 1057 (w), 1047 (w), 1030 (m), 992 (w), 970 (w), 947 (w), 933 (w), 896 (w), 848 (w), 815 (m), 802 (s), 766 (s), 708 (s), 678 (w) cm^{-1}.

2.3. *Preparation of [Co(D-cam)(3-pna)(H_2O)$_2$]$_n$ (2)*

$Co(NO_3)_2{\cdot}6H_2O$ (110 mg, 0.34 mmol), 3-pna (78 mg, 0.38 mmol), *D*-camphoric acid (76 mg, 0.38 mmol), and 0.5 mL of a 1.0 M NaOH solution were mixed with 10 mL of distilled H_2O in a 23 mL Teflon-lined acid digestion bomb. The bomb was sealed and heated in an oven at 120 °C for 24 h and then cooled slowly to 25 °C. Orange blocks of **2** (79 mg, 47% yield based on Co) were isolated after washing with distilled water, ethanol, and acetone and drying in air. $C_{21}H_{27}CoN_3O_7$ calcd C, 51.22; H, 5.53; N, 8.53%; found C, 51.06; H, 5.32; N, 8.30%. **IR** ($\tilde{\nu}$) = 3310 (w), 2977 (w), 1670 (w), 1651 (m), 1601 (w), 1585 (w), 1536 (s), 1477 (w), 1457 (w), 1432 (m), 1418 (m), 1390 (s), 1360 (m), 1332 (m), 1316 (w), 1288 (m), 1240 (w), 1197 (w), 1172 (w), 1124 (w), 1045 (w), 1031 (w), 999 (w), 941 (w), 896 (w), 872 (w), 848 (w), 825 (w), 806 (m), 791 (w), 745 (w), 697 (s) cm^{-1}.

2.4. *Preparation of [Ni(D-cam)(3-pna)(H_2O)$_2$]$_n$ (3)*

$Ni(NO_3)_2{\cdot}6H_2O$ (110 mg, 0.34 mmol), 3-pna (78 mg, 0.38 mmol), *D*-camphoric acid (76 mg, 0.38 mmol), and 1.0 mL of a 1.0 M NaOH solution were mixed with 10 mL of distilled H_2O in a 23 mL Teflon-lined acid digestion bomb. The bomb was sealed and heated in an oven at 120 °C for 24 h and then cooled slowly to 25 °C. Green blocks of **3** (83 mg, 50% yield based on Ni) were isolated after washing with distilled water, ethanol, and acetone and drying in air. $C_{21}H_{27}N_3NiO_7$ calcd C, 51.25; H, 5.53; N, 8.54%; found C, 52.17; H, 6.09; N, 8.30%. **IR** ($\tilde{\nu}$) = 3283 (m), 2923 (m), 1651 (m), 1600 (m), 1585 (m), 1525 (s), 1477 (m), 1431 (s), 1390 (s), 1360 (s), 1332 (m), 1287 (s), 1241 (m), 1197 (m), 1117 (m), 1049 (m), 1031 (m), 899 (m), 825 (m), 804 (m), 793 (m), 690 (s) cm^{-1}.

2.5. *X-ray crystallography*

Diffraction data for **1–3** were collected on a Bruker-AXS SMART-CCD X-ray diffractometer using graphite-monochromated Mo-K_α radiation ($\lambda = 0.71073$ Å) at 173 K. The data were processed via SAINT [28], and subjected to Lorentz and polarization effect and absorption corrections using SADABS [29]. The structures were solved using direct methods with SHELXTL [30]. All non-hydrogen atoms were refined anisotropically. Hydrogens bound to carbon were placed in calculated positions and refined isotropically with a riding model; those bound to nitrogen or oxygen were located by Fourier difference map, and restrained with isotropic displacement parameters. The 3-pna amide linkages in **2** and **3** were disordered equally over two sets of positions in a 50/50 ratio; these were modeled successfully using partial occupancies. Some distended thermal ellipsoids in the pyridyl rings of the 3-pna ligands in **2** and **3** are caused by unresolvable positional disorder. The Flack parameters [31] for **2** and **3** were 0.12(5) and 0.12(4), respectively, indicating a small amount of racemic twinning in both cases. The crystal structures of **2** and **3** were solved and refined in the acentric space group $P2_12_12_1$. Crystallographic details for **1–3** are given in table 1.

Table 1. Crystal and structure refinement data for **1–3**.

Data	1	2	3
Empirical formula	$C_{17}H_{11}CoN_3O_5S$	$C_{21}H_{27}CoN_3O_7$	$C_{21}H_{27}N_3NiO_7$
Formula weight	428.28	492.39	492.17
Crystal system	Triclinic	Orthorhombic	Orthorhombic
Space group	$P\bar{1}$	$P2_12_12_1$	$P2_12_12_1$
a (Å)	7.978(2)	7.2074(8)	7.2221(7)
b (Å)	10.331(3)	15.3888(17)	15.3429(15)
c (Å)	11.688(3)	18.909(2)	18.8605(18)
α (°)	64.068(3)	90	90
β (°)	73.732(3)	90	90
γ (°)	82.492(3)	90	90
V (Å^3)	831.5(4)	2097.3(4)	2089.9(4)
Z	2	4	4
D (g cm^{-3})	1.711	1.559	1.564
μ (mm^{-1})	1.194	0.869	0.979
Crystal size (mm)	0.18 × 0.07 × 0.03	0.29 × 0.23 × 0.14	0.43 × 0.22 × 0.11
Min./max. trans.	0.849	0.903	0.753
hkl ranges	$-8 \le h \le 9, -12 \le k \le 12, -14 \le l \le 13$	$-8 \le h \le 8, -18 \le k \le 18, -21 \le l \le 22$	$-8 \le h \le 8, -18 \le k \le 18, -22 \le l \le 22$
Total reflections	7974	16,171	16,833
Unique reflections	3089	3714	3825
R (int)	0.0686	0.0400	0.0296
Parameters	244	294	314
R_1[a] (all data)	0.1122	0.0684	0.0684
R_1[a] [$I > 2\sigma(I)$]	0.0556	0.0643	0.0644
wR_2[b] (all data)	0.1380	0.1816	0.1861
wR_2[b] [$I > 2\sigma(I)$]	0.1156	0.1782	0.1820
Max/min residual (e$^-$/Å^3)	0.601/−0.612	1.319/−0.618	1.473/−0.781
G.O.F.	1.017	1.078	1.057

[a]$R_1 = \Sigma||F_o| - |F_c||/\Sigma|F_o|$.
[b]$wR_2 = \{\Sigma[w(F_o^2 - F_c^2)^2]/\Sigma[wF_o^2]^2\}^{1/2}$.

3. Results and discussion

3.1. *Synthesis and infrared spectroscopy*

Compound **1** was prepared by hydrothermal reaction of cobalt nitrate, 3-pyridylnicotinamide, and 2,5-thiophenedicarboxylic acid. Compounds **2** and **3** were prepared by hydrothermal reaction of the requisite metal nitrate, 3-pyridylnicotinamide, and *D*-camphoric acid in the presence of additional base. Infrared spectra were consistent with the structural components as ascertained by X-ray diffraction. Broadened, weak bands at ~3200–3500 cm^{-1} signify the 3-pna amide N–H bonds, the water molecules of crystallization in **1**, or the aqua ligands in **2** and **3**. High-energy bands at ~2900–3000 cm^{-1} are attributed to C–H bond stretching modes in all cases. Asymmetric and symmetric C–O stretching modes of the dicarboxylate ligands are indicated by slightly broadened, strong bands at 1548 and 1372 cm^{-1} (**1**), 1536 and 1390 cm^{-1} (**2**), and 1525 and 1390 cm^{-1} (**3**). Sharp, medium-intensity bands in the range of ~1600 cm^{-1} to ~1200 cm^{-1} are ascribed to stretching modes of the pyridyl rings of the 3-pna ligands (for all) and the aromatic rings of the tpdc ligands (for **1**) [32]. Features corresponding to pyridyl and aryl ring puckering are observed between 800 and 600 cm^{-1}. Sharp, moderate-intensity bands at 1673 cm^{-1} (**1**), 1651 cm^{-1} (**2**), and 1651 cm^{-1} (**3**) signify the presence of the amide C=O bond within the 3-pna ligands. IR spectra for **1–3** are shown in figures S1–S3 (see online supplemental material at http://dx.doi.org/10.1080/00958972.2015.1038997).

3.2. *Structural description of [Co(tpdc)(3-pna)]$_n$ (1)*

The asymmetric unit of **1** consists of a divalent cobalt, a 3-pna ligand, and a tpdc ligand [figure 1(a)]. A distorted trigonal bipyramidal $\{CoN_2O_3\}$ coordination environment is

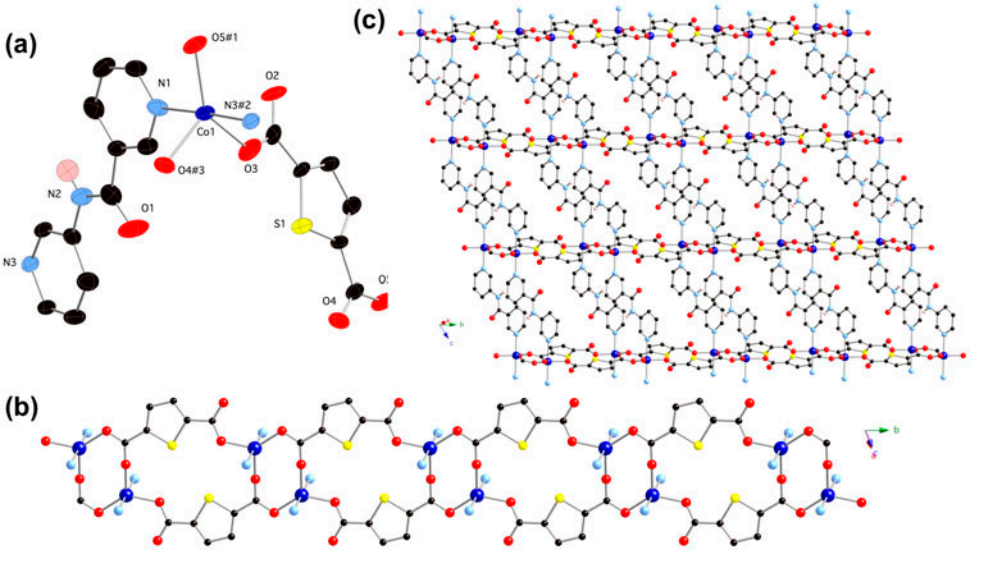

Figure 1. (a) Distorted trigonal bipyramidal coordination environment of **1**. Thermal ellipsoids are shown at 50% probability. Most hydrogens are omitted for clarity. (b) $[Co(tpdc)]_n$ 1-D chain motif in **1**, featuring embedded $\{Co_2(OCO)_2\}$ dinuclear units. (c) 2-D $[Co(tpdc)(3\text{-pna})]_n$ coordination polymer layer in **1**.

Table 2. Selected bond distance (Å) and angle (°) data for **1**.

Co1–O5$^{\#1}$	2.010(3)	O3–Co1–O5$^{\#1}$	134.77(17)
Co1–N3$^{\#2}$	2.153(4)	O3–Co1–N3$^{\#2}$	88.04(15)
Co1–O3	1.976(3)	O3–Co1–O4$^{\#3}$	98.50(16)
Co1–O4$^{\#3}$	2.008(4)	O3–Co1–N1	91.39(16)
Co1–N1	2.184(4)	O4$^{\#3}$–Co1–O5$^{\#1}$	126.56(15)
O5$^{\#1}$–Co1–N3$^{\#2}$	94.09(15)	O4$^{\#3}$–Co1–N3$^{\#2}$	91.08(16)
O5$^{\#1}$–Co1–N1	87.90(15)	O4$^{\#3}$–Co1–N1	86.79(16)
N3$^{\#2}$–Co1–N1	177.70(16)		

Notes: Symmetry transformations: #1x, y + 1, z; #2x–1, y, z + 1; #3–x + 1, –y + 1, –z + 1.

observed at cobalt ($\tau = 0.71$) [33], with pyridyl nitrogen donors from two 3-pna ligands in the axial positions. Carboxylate oxygen donors from three different tpdc ligands occupy the equatorial plane. Bond lengths and angles within the relatively uncommon five-coordinated cobalt environment are listed in table 2.

The tpdc ligands in **1** adopt an exotridentate μ_3-κ^3O:O′:O″ binding mode, with one carboxylate oxygen remaining unligated (Co···O distance = 3.184 Å). The carboxylate groups without unligated oxygen atoms form dinuclear units featuring eight-membered $\{Co_2(OCO)_2\}$ rings, via a *syn–anti* interaction. The Co···Co through-space distance across the eight-membered rings measures 3.839 Å. The full span of the tpdc ligands connects these dinuclear units into $[Co(tpdc)]_n$ 1-D chain patterns that are oriented along the *b*-axis [figure 1(b)]. The closest interdimer Co···Co contact measures 7.884 Å, across $\{Co_2(OC_2SC_2O)_2\}$ 16-membered rings.

Pairs of tethering *anti* conformation 3-pna ligands connect $\{Co_2(OCO)_2\}$ dinuclear units in neighboring $[Co(tpdc)]_n$ 1-D chain motifs, forming 2-D $[Co(tpdc)(3\text{-pna})]_n$ coordination polymer layer patterns [figure 1(c)]. These are oriented parallel to the (1 0 1) crystal planes. The Co···Co distance through the span of the 3-pna ligands measures 12.166 Å. Treating the exotridentate tpdc ligands as 3-connected nodes and the cobalt ions as 5-connected nodes allows a 3,5-connected topology to be invoked for the layer motif of **1** (figure 2).

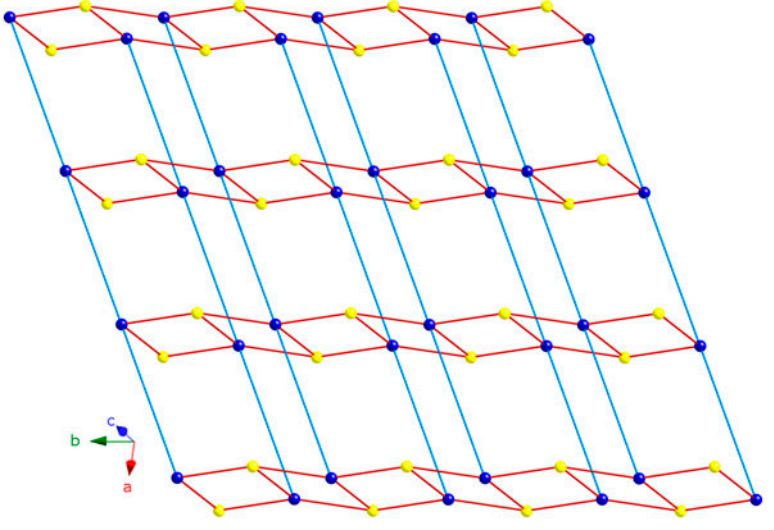

Figure 2. Schematic perspective of the 3,5-connected layer topology of **1**.

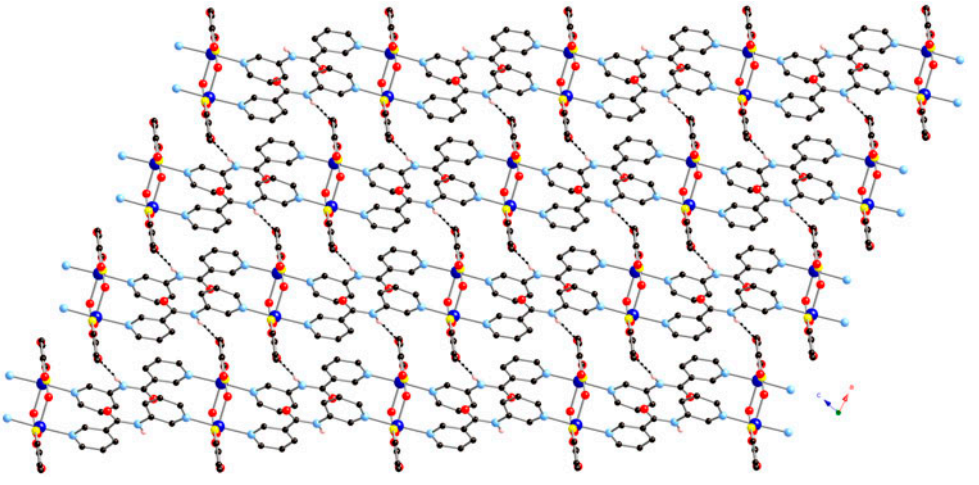

Figure 3. Stacking of layer motifs in **1**.

According to TOPOS [34], the Schläfli symbol for this network is $(4^26)(4^{2\cdot}6^78)$, also known as the 3,5L2 topology. Previous examples of this topology include [Zn(5-methoxyisophthalate) (dipyridylethylene) (DMF)]$_n$ [35] and the more closely related [Ni(ip)(bpy)]$_n$ [36].

Hydrogen-bonding donation from the N–H bonds of the 3-pna amide moieties to unligated tpdc carboxylate oxygens in neighboring layers provides the supramolecular impetus for construction of the 3-D crystal structure of 1 (table S1). Adjacent layers stack in a direct *AAA* pattern along the *a*-axis (figure 3). The close stacking of neighboring layers does not provide incipient void space necessary to host water molecules of crystallization or other unligated species.

3.3. *Structural description of [Co(D-cam)(3-pna)(H$_2$O)$_2$]$_n$ (2) and [Ni(D-cam)(3-pna)(H$_2$O)$_2$]$_n$ (3)*

As **2** and **3** are isostructural, only the single-crystal structure of **2** will be discussed in detail. Compound **2** crystallizes in the acentric orthorhombic space group $P2_12_12_1$ with an asymmetric unit consisting of a divalent cobalt atom, a *D*-cam ligand, a 3-pna ligand, and two bound water molecules. The coordination environment at cobalt is a distorted $\{CoO_4N_2\}$ octahedron with 3-pna pyridyl donors in *trans* positions [figure 4(a)]. Water ligands are located in *trans* coordination sites, as well as carboxylate oxygens belonging to two *D*-cam ligands. Pertinent bond information for **2** and **3** is listed in table 3. The slight lengthening of all the bond lengths in **2** with respect to **3** is consistent with well-known ionic radius trends [37]. Compounds **2** and **3** are also isostructural with their cadmium congener, [Cd(*D*-cam)(3-pna)(H$_2$O)$_2$]$_n$ [14].

In contrast to the exotridentate binding mode of the tpdc ligands in **1**, the *D*-cam ligands in **2** adopt a simple bis(monodentate) binding mode between neighboring cobalt ions. The *D*-cam ligands therefore form 1-D [Co(*D*-cam)(H$_2$O)$_2$]$_n$ chains oriented along the *c*-axis, with a Co···Co through-ligand distance of 9.456 Å. These Co···Co spans are also bridged by *syn* conformation 3-pna ligands, giving 1-D [Co(*D*-cam)(3-pna)(H$_2$O)$_2$]$_n$ chain motifs [figure 4(b)]. Hydrogen bonding provided by the aqua ligands prevents ligation of half of

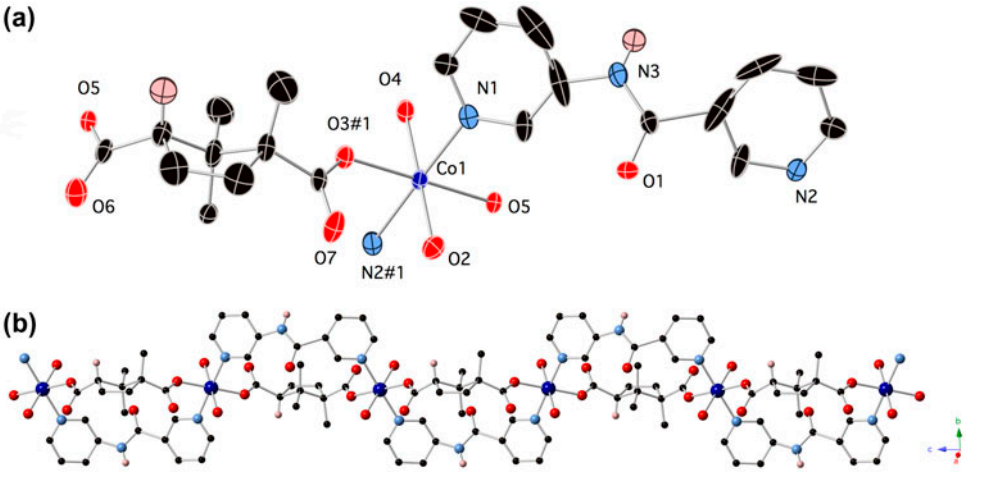

Figure 4. (a) Distorted octahedral coordination environment of **2**. Thermal ellipsoids are shown at 50% probability. Most hydrogens are omitted for clarity. (b) $[Co(D\text{-cam})(3\text{-pna})(H_2O)_2]_n$ 1-D chain motif in **2**.

Table 3. Selected bond distance (Å) and angle (°) data for **2** and **3**.

Co1–O5	2.065(4)	Ni1–O7	2.049(4)
Co1–O3$^{\#1}$	2.071(4)	Ni1–O3$^{\#2}$	2.054(4)
Co1–O2	2.101(4)	Ni1–O5	2.080(4)
Co1–N2$^{\#1}$	2.166(5)	Ni1–O6	2.086(4)
Co1–O4	2.107(4)	Ni1–N3	2.122(5)
Co1–N1	2.167(5)	Ni1–N2$^{\#3}$	2.124(5)
O5–Co1–O3$^{\#1}$	179.06(18)	O7–Ni1–O3$^{\#2}$	178.94(18)
O5–Co1–O2	91.09(16)	O7–Ni1–O5	89.86(16)
O5–Co1–N2$^{\#1}$	88.35(17)	O3$^{\#2}$–Ni1–O5	90.67(16)
O5–Co1–O4	89.83(16)	O7–Ni1–O6	90.70(17)
O5–Co1–N1	90.40(16)	O3$^{\#2}$–Ni1–O6	88.78(16)
O3$^{\#1}$–Co1–O2	89.45(16)	O5–Ni1–O6	179.44(17)
O3$^{\#1}$–Co1–N2$^{\#1}$	90.93(17)	O7–Ni1–N3	88.01(17)
O3$^{\#1}$–Co1–O4	89.64(16)	O3$^{\#2}$–Ni1–N3	91.11(17)
O3$^{\#1}$–Co1–N1	90.32(16)	O5–Ni1–N3	85.97(19)
O2–Co1–N2$^{\#1}$	86.04(18)	O6–Ni1–N3	94.13(18)
O2–Co1–O4	178.94(17)	O7–Ni1–N2$^{\#3}$	90.76(16)
O2–Co1–N1	94.17(18)	O3$^{\#2}$–Ni1–N2$^{\#3}$	90.11(16)
N2$^{\#1}$–Co1–N1	178.73(19)	O5–Ni1–N2$^{\#3}$	94.42(18)
O4–Co1–N2$^{\#1}$	94.52(18)	O6–Ni1–N2$^{\#3}$	85.49(18)
O4–Co1–N1	85.28(18)	N3–Ni1–N2$^{\#3}$	178.71(19)

Notes: Symmetry transformations: $^{\#1}-x + 1/2, -y, z-1/2$; $^{\#2}-x + 1/2, -y + 1, z-1/2$; $^{\#3}-x + 1/2, -y + 1, z + ½$.

the *D*-cam carboxylate oxygens (table S1). Adjacent chains aggregate into supramolecular layers in the *ac* crystal planes, by means of O–H···O hydrogen-bonding donation from water ligands to unligated *D*-cam carboxylate oxygens. These layers then further aggregate by N–H···O hydrogen bonding between 3-pna N–H bonds in one supramolecular layer and 3-pna carbonyl groups in another layer. Each chain motif in **2** therefore engages in hydrogen bonding to six others (figure S4).

3.4. *Thermal properties*

Thermogravimetric analysis was carried out on samples of **1** and **2** under flowing nitrogen to investigate their degradation behavior. The mass of **1** remained largely stable until ~325 °C, whereupon ligand combustion occurred; its final mass remnant of 11.2% at 600 °C is roughly consistent with that expected of Co metal (13.8% calcd). For **2**, its water ligands were ejected in the temperature regime from ~150 to ~180 °C, with a mass loss of 7.7% closely corresponding with that expected for elimination of two molar equivalents of water (7.3% calcd). Ligand ejection occurred in several stages between ~180 and ~450 °C, with a final mass remnant at 600 °C of 12.9% matching well with deposition of Co metal (12.0% calcd). Thermogravimetric analysis plots for **1** and **2** are shown in figures S5 and S6, respectively.

3.5. *Magnetic study for 1*

A variable-temperature magnetic susceptibility study was undertaken to investigate magnetic interactions within the *syn–anti* carboxylate bridged $\{Co_2(OCO)_2\}$ rings in **1**. The $\chi_m T$ product of 2.40 $cm^3\,K\,mol^{-1}$ Co at 300 K is higher than that expected for a spin-only $S = 3/2$ ion because of the spin–orbit coupling to coordinated divalent cobalt ions [38]. A slow decrease in $\chi_m T$ occurs between 300 and 100 K, at which point it reaches 2.34 $cm^3\,K\,mol^{-1}$ Co. Below 100 K, the $\chi_m T$ product decreases more rapidly, reaching 1.59 $cm^3\,K\,mol^{-1}$ Co at 2 K. The shape of the $\chi_m T(T)$ graph (figure 5) is ascribed to antiferromagnetic coupling between paramagnetic cobalt ions and the population of Kramers doublet $S = 1/2$ states [38]. The magnetic data were fit to Rueff's phenomenological expression [39] (equation (1)), which takes magnetic superexchange (J) and single-ion effects such as zero-field splitting (D) into account. The best fit values were $A = 0.77(2)$, $B = 1.70(1)$, with $C = 2.47(2)$

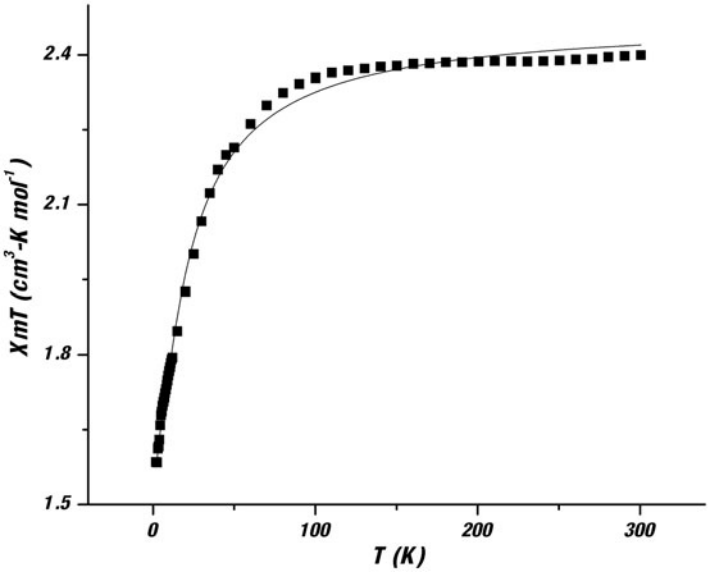

Figure 5. $\chi_m T$ *vs.* T plot for **1**. The dark line represents the best fit to equation (1).

giving $g = 2.29(2)$, $D = 14.4(6)$ cm^{-1}, and $J = -0.10(2)$ cm^{-1} with $R = \{\Sigma[(\chi_m T)_{obs} - (\chi_m T)_{Calcd}]^2\}^{1/2} = 3.2 \times 10^{-4}$. The negative, small value of J corroborates the presence of weak antiferromagnetic coupling between the cobalt ions in the $\{Co_2(OCO)_2\}$ dimeric units. In **1**, the 3-pna ligand and the full span of the tdc ligands are too lengthy to moderate any tangible spin communication. A field-dependent study at 2 K for the magnetization of **1** did not reveal any hysteresis, so alternating current experiments were not undertaken.

$$\chi_m T = A \exp(-D/kT) + B \exp(J/kT)$$

$$\text{where } A + B = C = (5Ng^2\beta^2 \ / \ 4k) \tag{1}$$

5. Conclusion

Divalent cobalt coordination polymers have been synthesized by employing the conformationally flexible hydrogen-bonding capable 3-pyridylnicotinamide ligand, in tandem with an organic dicarboxylate containing five-membered ring units. In the case of the aromatic 2,5-thiophenedicarboxylate, with a flat five-membered central ring, the resulting coordination polymer manifested a dimer-based 3,5-connected 2-D layer topology with *anti* conformation 3-pna ligands. The aliphatic five-membered ring in *D*-camphorate positions both of the carboxylate groups on one side of the ring plane, resulting in a curled disposition of the two donors relative to each other. In turn, this instilled a chain motif for the resulting coordination polymer, supported by bridging *syn* conformation 3-pna ligands that could span the same metal–metal distance as the camphorate ligands. The hydrogen-bonding facility and conformational flexibility of 3-pna ligands provided a supramolecular structure-directing effect in both cases. The ligand-based changes in dimensionality also cause physical property changes, as the 2-D net of **1** proved to be much more thermally stable than the 1-D chains of **2**.

Supplementary material

Additional molecular graphics, TGA traces, and hydrogen-bonding information. Crystallographic data (excluding structure factors) for **1–3** have been deposited with the Cambridge Crystallographic Data Center with CCDC Nos. 1007455–1007457. Copies of the data can be obtained free of charge via the Internet at https://summary.ccdc.cam.ac.uk/structure-summary-form.

Acknowledgements

We thank Dr Rui Huang and Ms Jessica Goldsworthy for experimental assistance.

Disclosure statement

No potential conflict of interest was reported by the authors.

Funding

This work was supported by the Lyman Briggs College of Michigan State University.

References

[1] L.J. Murray, M. Dincă, J.R. Long. *Chem. Soc. Rev.*, **38**, 1294 (2009), and references therein.
[2] J.R. Li, R.J. Kuppler, H.C. Zhou. *Chem. Soc. Rev.*, **38**, 1477 (2009), and references therein.
[3] (a) M. Plabst, L.B. McCusker, T. Bein. *J. Am. Chem. Soc.*, **131**, 18112 (2009); (b) Y. Liu, V.C. Kravtsov, M. Eddaoudi. *Angew. Chem. Int. Ed.*, **47**, 8446 (2008); (c) F. Nouar, J. Eckert, J.F. Eubank, P. Forster, M. Eddaoudi. *J. Am. Chem. Soc.*, **131**, 10394 (2009).
[4] (a) J. Lee, O.K. Farha, J. Roberts, K.A. Scheidt, S.T. Nguyen, J.T. Hupp. *Chem. Soc. Rev.*, **38**, 1450 (2009), and references therein; (b) L. Ma, C. Abney, W. Lin. *Chem. Soc. Rev.*, **38**, 1248 (2009), and references therein.
[5] G. Wang, L. Yang, Y. Li, H. Song, W. Ruan, Z. Chang, X. Bu. *Dalton Trans.*, **42**, 12865 (2013).
[6] L. Carlucci, G. Ciani, D.M. Proserpio. *Coord. Chem. Rev.*, **246**, 247 (2003) and references therein.
[7] (a) P. Lightfoot, A.J. Snedden. *J. Chem. Soc., Dalton Trans.*, 3549, (1999); (b) X. Wang, C. Qin, E. Wang, L. Xu. *J. Mol. Struct.*, **737**, 49 (2005); (c) E. Suresh, K. Boopalan, R.V. Jasra, M.M. Bhadbhade. *Inorg. Chem.*, **40**, 4078 (2001); (d) H. Xu, R. Sun, Y.Z. Li, J.F. Bai. *Acta Crystallogr., Sect. C*, **62**, m1156 (2006).
[8] (a) M. Eddaoudi, J. Kim, N. Rosi, D. Vodak, J. Wachter, M. O'Keeffe, O.M. Yaghi. *Science*, **295**, 469 (2002); (b) X.-N. Cheng, W.-X. Zhang, Y.-Y. Lin, Y.-Z. Zheng, X.-M. Chen. *Adv. Mater.*, **19**, 1494 (2007).
[9] (a) J. Tao, M.L. Tong, X.M. Chen. *J. Chem. Soc., Dalton Trans.*, 3669, (2000); (b) Y. Wen, J. Cheng, Y. Feng, J. Zhang, Z. Li, Y. Yao. *Inorg. Chim. Acta*, **358**, 3347 (2005); (c) J. Song, J. Lu, Y. Chen, Y. Liu, R. Zhou, X. Xu. *J. Xu. Inorg. Chem. Commun.*, **9**, 1079 (2006).
[10] (a) B. Chen, C. Liang, J. Yang, D.S. Contreras, Y.L. Clancy, E.B. Lobkovsky, O.M. Yaghi, S. Dai. *Angew. Chem., Int. Ed.*, **45**, 1390 (2006); (b) S.W. Lee, H.J. Kim, Y.K. Lee, K. Park, J.H. Son, Y. Kwon. *Inorg. Chim. Acta*, **353**, 151 (2003).
[11] J.W. Uebler, A.L. Pochodylo, R.J. Staples, R.L. LaDuca. *Cryst. Growth Des.*, **13**, 2220 (2013).
[12] J.W. Uebler, A.L. Pochodylo, R.L. LaDuca. *Inorg. Chim. Acta*, **405**, 31 (2013).
[13] J.S. Goldsworthy, R.J. Staples, R.L. LaDuca. *J. Mol. Struct.*, **1062**, 116 (2014).
[14] J.A. Wilson, R.L. LaDuca. *Inorg. Chim. Acta*, **403**, 136 (2013).
[15] J.W. Uebler, J.A. Wilson, R.L. LaDuca. *CrystEngComm*., **15**, 5218 (2013).
[16] J.E. Mizzi, R.L. LaDuca. *Inorg. Chim. Acta*, **411**, 188 (2014).
[17] S.H. Qiblawi, A.L. Pochodylo, R.L. LaDuca. *CrystEngComm.*, **15**, 8979 (2013).
[18] P.E. Kraft, J.E. Mizzi, R.L. LaDuca. *Inorg. Chim. Acta*, **409**, 449 (2014).
[19] S.H. Qiblawi, R.L. LaDuca. *Inorg. Chim. Acta*, **413**, 115 (2014).
[20] D. Kumar, A. Das, P. Dastidar. *Cryst. Growth Des.*, **6**, 1903 (2006).
[21] L. Zhou, C. Wang, X. Zheng, Z. Tian, L. Wen, H. Qua, D. Li. *Dalton Trans.*, **42**, 16375 (2013).
[22] L. Song, C. Jiang, C. Jiao, J. Zhang, L. Sun, F. Xu, W. You, Z. Wang. *J. Zhao. Cryst. Growth Des.*, **10**, 5020 (2010).
[23] H. Jia, W. Li, Z. Ju, J. Zhang. *Eur. J. Inorg. Chem.*, 4264, (2006).
[24] J. Zhang, E. Chew, S. Chen, J.T.H. Pham, X. Bu. *Inorg. Chem.*, **47**, 3495 (2008).
[25] J. Zhang, X. Bu. *Angew. Chem., Int. Ed.*, **46**, 6115 (2007).
[26] K.M. Blake, C.M. Gandolfo, J.W. Uebler, R.L. LaDuca. *Cryst. Growth Des.*, **12**, 5125 (2012).
[27] T.S. Gardner, E. Wenis, J.J. Lee. *J. Org. Chem.*, **19**, 753 (1954).
[28] SAINT, *Software for Data Extraction and Reduction (Version 6.02)*, Bruker AXS, Inc., Madison, WI (2002).
[29] SADABS, *Software for Empirical Absorption Correction (Version 2.03)*, Bruker AXS, Inc., Madison, WI (2002).
[30] G.M. Sheldrick. *SHELXTL, Program for Crystal Structure Refinement*, University of Gottingen, Germany (1997).
[31] H.D. Flack. *Acta Crystallogr. A*, **29**, 876 (1983).
[32] M. Kurmoo, C. Estournes, Y. Oka, H. Kumagai, K. Inoue. *Inorg. Chem.*, **44**, 217 (2005).
[33] A.W. Addison, T.N.J. Rao, J. Reedijk, J. van Rijn, G.C. Verschoor. *J. Chem. Soc., Dalton Trans.*, 1349, (1984).
[34] V.A.Blatov, A.P.Shevchenko, D.M.Proserpio. *Cryst. Growth Des*., **14**, 3576 (2014). TOPOS software is available for download at: http://www.topos.ssu.samara.ru.
[35] H. Sato, R. Matsuda, M. Mir, S. Kitagawa. *Chem. Commun.*, **48**, 7919 (2012).
[36] J. Tao, X. Chen, R. Huang, L. Zheng. *J. Solid State Chem.*, **170**, 130 (2003).
[37] R.D. Shannon. *Acta Crystallogr. A*, **32**, 751 (1976).
[38] O. Kahn. *Molecular Magnetism*., VCH Publishers, New York, NY (1993).
[39] J.M. Rueff, N. Masciocchi, P. Rabu, A. Sironi, A. Skoulios. *Eur. J. Inorg. Chem.*, 2843, (2001).